

# Single-layer Deposits of Nickel Base Superalloy by means of Selective Laser Melting

Jorge A. Ramos, Jeremy Murphy, Karmen Lappo  
Kristin Wood, David L. Bourell, Joseph J. Beaman

Laboratory for Freeform Fabrication  
The University of Texas at Austin, TX 78712

## Abstract

Single layer deposits consisting of Mar-M 247 powder were consolidated on Alloy 718 polycrystalline flat sheets by means of the Selective Laser Melting (SLM) technique. The deposition process consisted in selectively fusing a powder bed pre-compacted using of an insulating non-wettable mask trough. The mask-powder-substrate arrangement was pre-heated inside a processing chamber under high vacuum. An inert-reducing atmosphere was applied, and a focused Nd:YAG laser beam was then raster scanned at high speed along the contour of the trough, providing energy to induce a melting front to propagate along the powder as well as over the surface of the plate. As the laser beam moved forward a solidification front was left behind with a metallurgical bond between the substrate and the deposited layer. Optical microscopy revealed that epitaxial growth occurred in the [001] direction from the melted substrate to about half the height of the deposits. Above that height, the [001] dendritic front bowed towards the [100] direction. A dendritic-equiaxed transition appeared near the free surface of the deposit. These results indicate that the SLM technique could have potential application for growing single crystal structures as well as in repairing damaged or worn turbine blades.

## Introduction

Surface melting of a material can be readily achieved by a continuous traveling heat source (e.g., a high-power focused laser beam), the bulk acting as a heat sink during the solidification stage. The resulting solidified material has the same chemical composition of the parent material. Nonetheless, if a high solidification rate is attained, it may produce a different microstructure with enhanced mechanical properties. A common practice is to pre-place or inject an alloy powder at the surface of the material prior or during the surface melting process to alter the chemical composition of the melt pool. Another variation is to melt a different material placed on the surface so that mixing with the substrate material is limited to the minimum required to produce effective bonding. When a laser beam is employed as the heat source, the latter two laser melting techniques are referred respectively as laser alloying and laser cladding<sup>1-3</sup>.

In 1998 Das *et al.*<sup>4</sup> developed a technique for the production of abrasive turbine blade tips based on selective laser melting a pre-placed layer of material along the contour of the tip. Direct laser fabrication of components was achieved from a bed of loose cermet powder consisting of Mar-M 247 nickel superalloy matrix (73 wt.%) mixed with Ti coated cubic boron nitride (9 wt.%) and Ti coated alumina (18 wt.%). The powders were mechanically blended, poured into molds and leveled to ensure constant layer thickness. Tip shape processing was done by two alternative methods. The first method consisted in selectively laser raster scanning the shape of the blade tip out of a powder bed container. The second method was to laser process a rail-shaped tip from powder contained in a mold. In both cases, the powder was processed successfully under high vacuum ( $< 10^{-5}$  Torr) within an energy density window of 2400-3878 J/cm<sup>2</sup>. It was observed that the mold material affected the thermal profile generated and thus the solidification microstructure of the component. Ceramic containers insulated the bottom surface of the powder bed and set up a uniform thermal gradient resulting in partially directional solidification or equiaxed growth. Steel and superalloy containers produced fine dendrite spacing in the solidification microstructure.

Gäumann *et al.*<sup>5</sup> in 1999 developed a laser cladding technique called Epitaxial Laser Metal Forming (E-LMF) that combines the advantages of near net shape manufacturing with close control of the solidification microstructure. When laser power and solidification rates are precisely controlled, columnar dendritic growth can be stabilized, thereby avoiding nucleation and growth of equiaxed grains in the laser clad. In this manner it is feasible to deposit a single crystal clad by epitaxial growth onto a single crystal substrate. A fine dendritic morphology with low residual porosity is achieved due to the high solidification rates and temperature gradients reached during the process. This methodology was demonstrated using CMSX-4 superalloy powder over single crystal substrates of the same material. The volume fraction of equiaxed grains  $\phi$  ahead of the solid-liquid interface was calculated numerically as a function of solidification conditions: thermal gradient in the liquid  $G_L$ , local solidification rate  $R_L$ , density of nucleation sites  $N_0$  and nucleation undercooling  $\Delta T_n$ . The  $\phi$  parameter determined the columnar to equiaxed transition (CET) and it must be less than 0.66% to assure columnar growth. It was determined for this alloy that the critical value of  $N_0$  and  $\Delta T_n$  corresponded to respectively to is  $2 \times 10^{15} \text{ m}^{-3}$  and 2.5 °C, for high values of  $G_L$ . Micrographs showed that initially, the primary growth direction of the dendrites was perpendicular to the substrate and there was a systematic change in growth morphology close to the surface of the clad, due to a change in dendrite growth direction. The columnar growth of the dendrites was suddenly altered at about half the height of the clad. An electron back scattered diffraction (EBSD) map showed no signs of other grains at this location. This new growth morphology was due to a tilting of the primary growth direction by 90° due to a change in the shape of the isotherms, where dendrite arms of the columnar dendrites changed into dendrite trunks. Nonetheless, some grains appearing at the surface of the clad were due partly to the changing solidification conditions at the edge of the clad. That is, the thermal gradient was reduced and the solidification rate increased. Impingement of powder particles that might not be completely molten at the surface can also affect the number of nucleation sites favoring the CET. The primary arm spacing in the deposits corresponded to 11  $\mu\text{m}$ .

The objective of the present research is to build up the knowledge and capability for restoration of Ni-base superalloy single crystal components (e.g. aircraft combustion engine turbine blades) to near original properties and dimensions at a small fraction of the cost of replacing the blades. Selective laser melting (SLM) is the chosen technology to perform this restoration due to the hardware availability and previous research experience (Ref.4). As mentioned before, it is crucial to develop the ability to tailor the microstructure of the deposited materials as it is being laid. Complete epitaxial growth from the substrate material into the solidifying deposited layer is the main requirement. In the present research single-track, single-layers of Mar-M 247 material were successfully deposited over polycrystalline Ni-base Alloy 718 flat sheets by means of mask confinement of the alloy powder followed by SLM. Single-layer deposits having a U-shape wall were achieved this way as well. Feasibility of epitaxial solidification growth within the deposits was demonstrated.

### Selective Laser Melting Process Schematics

The mask confines the superalloy powder along the geometry and provides minimum lateral heat loss. It is coated with a “stop-off” layer of boron nitride to protect it from eventual laser beam interaction and to provide a non-wettable surface to the molten alloy allowing easy detachment once the deposit has solidified. Figure 1 illustrates the configuration of the mask-powder-substrate assembly and the SLM process. The laser beam raster scans back and forth laterally and travels along the mask trough, melting the entire powder depth and a small fraction of the substrate. As the melt pool advances its tail solidifies forming a sound metallurgical bonding with the substrate. The substrate rests on top of a vertical wall placed immediately below the confined powder is, as seen in Figure 2. This wall acts as one-directional heat sink so that heat extraction during the solidification is one-dimensional along the z-direction enhancing solidification growth in the negative z-direction.

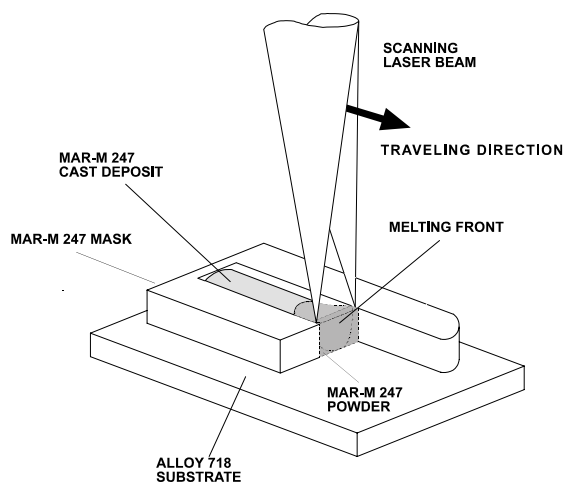


Figure 1. Overall schematics of the mask-powder-substrate arrangement during selective laser melting.

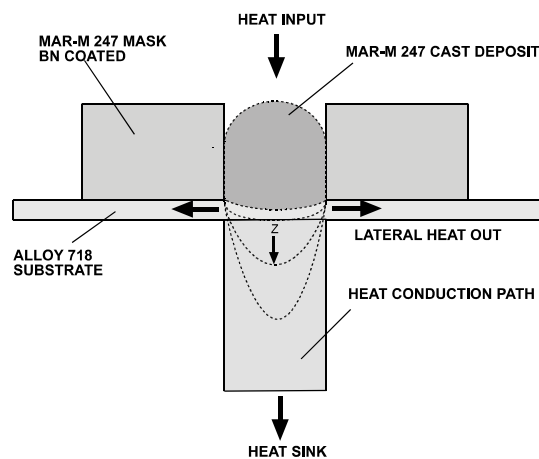


Figure 2. Cross-section schematic of the mask-powder-substrate arrangement indicating major heat flow paths.

Figure 3 illustrates the CAD drawing of the registration fixture for the mask and substrate plate. It provides a robust clamping system for two masks, higher alignment accuracy and thus enhanced process repeatability. It also allows for heat conduction to take place preferentially through a wall boundary, in an attempt to anticipate the direct growth of a blade tip from a parent blade. Figure 4 shows the as-built fixture having two insulating masks registered. Reduction of far-field temperature gradients in the substrate plate is also obtained minimizing residual stresses and warping.

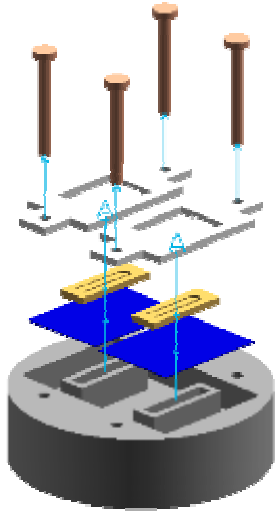


Figure 3. CAD representation of the registration fixture assembly



Figure 4. Registration fixture as-built, containing U-shape masks and Alloy 718 substrate plates.

### Solidification Mechanics during SLM

When a laser beam moves over the surface of a material, along a straight path with constant traveling speed and with enough power to cause melting, a dynamic thermal equilibrium between heat supply and heat extraction is established<sup>2,3,5-7</sup>. Under this pseudo-steady-state condition, the shape of the molten pool remains constant for any given laser traveling speed  $v_t$ <sup>2,3,6,7</sup>. The shape of the melting pool is also a function of the laser power  $P$  and speed as well as the thermal diffusivity of the material. High speed and power and low thermal diffusivity promote the formation of a “comet-shaped” melting pool, whereas low speed and power and high thermal diffusivity provide the conditions for a spherical shaped melt pool. Others factors that determine the shape of the fusion zone are convection due to buoyancy, surface tension gradient and electromagnetic forces<sup>6</sup>.

During solidification of the melt pool, growth of the columnar grains proceeds closely to the direction of the maximum thermal gradient in the molten pool, i.e., normal to the fusion boundary<sup>5-7</sup>. The columnar grain morphology thus depends on the molten pool geometry. A spherically shaped melt pool will reveal curved and tapered columnar grains owing to a shift in the direction of the maximum thermal gradient in the liquid

from the fusion boundary towards the liquid free surface. In contrast, a comet-shaped melt pool produces straight and broad columnar grains, as the direction of the maximum temperature gradient in the melt does not change significantly during the solidification process<sup>6</sup>.

The growth rate  $R$  of the columnar grains is also geometrically related to the traveling speed of the heat source and the shape of the fusion zone. Since the shape of the melt pool remains constant during the pseudo-steady-state,  $R$  varies with position along the fusion boundary. At each position along the fusion boundary, the columnar grains grow parallel with respect to the thermal gradient in the melt pool. If the angle between the growth direction and the laser beam traveling speed direction is taken as  $\theta$  then the steady state nominal growth rate  $R_N$  becomes<sup>3,5-7</sup>,

$$R_N = v_t \cos \theta \quad (1)$$

In cubic metals and alloys, the  $\langle 100 \rangle$  direction corresponds to the major dendrite growth direction<sup>5-7</sup>. Because of the existence of preferred growth directions, the local growth rate of the crystals  $R_L$  will always be higher than the nominal rate,  $R_N$ . If  $\phi$  is the angle between the fusion boundary normal and the  $\langle 100 \rangle$  direction, then the relationship between  $R_L$  and  $R_N$  is given by,

$$R_L = R_N / \cos \phi \quad (2)$$

$R_L$  will increase with increasing misalignment of the crystal with respect to the direction of the maximum thermal gradient in the melt zone. However, misaligned grains require an increase in the undercooling ahead of the solid/liquid interface; they will be outgrown by grains that have an orientation closer to that of the maximum thermal gradient<sup>6</sup>.

### Solidification growth stability

The stability of the solidification front is controlled by the extent of the constitutional undercooling ahead of the advancing interface. It is influenced by factors such as the alloying or impurity elements presence, local growth rate  $R_L$ , and thermal gradient in the melt zone  $G_L$ . A high  $G_L/R_L$  ratio provides a planar solidification front. At lower  $G_L/R_L$  ratio, the morphology changes to cellular, cellular-dendritic or dendritic depending on the degree of constitutional undercooling ahead of the advancing front<sup>6,7</sup>.

Normally in SLM, the  $G_L/R_L$  ratio at the fusion boundary is large enough to facilitate planar solidification. The temperature gradient in the melt zone decreases with distance from the fusion boundary and a cellular-dendritic type of substructure is observed in the central areas of the melt pool. The substructure may change from dendritic to equiaxed close to the free surface if the degree of constitutional undercooling in front of the advancing interface is sufficiently large<sup>5-7</sup>.

### Columnar growth reorientation

A columnar grain can adjust its orientation during solidification to accommodate a shift in the direction of the maximum temperature gradient in the melt pool by means of two mechanisms: bowing or re-nucleation.

During bowing, a continuous change in the crystal orientation will result in curved columnar grains. The adjustment of the crystal orientation is promoted by multiple branching of dendrites present within the grains. Alternatively, the reorientation can be accommodated by the presence of defects at the solid/liquid interface, e.g. screw dislocations, twin boundaries, rotation boundaries, etc. Under these circumstances, the growth rate of the dendrites will never exceed the laser beam traveling speed,  $v_t$ <sup>5-7</sup>.

Under the second mechanism, heterogeneous nucleation is the main driving force since the fused metal often contains a high number of second phase particles. Reorientation of the columnar grains will occur when the cell/dendrite alignment angle reaches a critical value that depends on the nucleation potency of the catalyst particles. Nucleation of new grains ahead of the advancing columnar interface can also occur from random solid dendrite fragments contained in the melt pool. Alternatively, since the partially melted base grains at the fusion boundary are loosely held together by the liquid between them, there is a possibility that some of these grains may detach themselves from the base metal and be trapped in the solidification front. Like dendrite fragments, such partially melted grains can act as seed crystals<sup>6</sup>.

### Columnar to equiaxed transition

An equiaxed zone is often observed close to the free surface of the melt pool. The melt becomes undercooled by the extensive segregation of solute where the growing solidification front impinges. This makes the crystals hotter than the liquid and gives rise to radial heat flow away from the crystals in the same direction as that of growth<sup>5,6</sup>. For a given alloy system containing a fixed number of heterogeneous nucleation sites, it is reasonable to assume that the columnar to equiaxed transition occurs when the  $G_L/R_L$  ratio drops below a certain critical value  $f$ <sup>6</sup>, this is,

$$f_{\text{critical}} > G_L/R_L \quad (3)$$

Figure 5 illustrates the selective laser melting of a layer of pre-placed powder over a substrate under pseudo-steady-state thermal conditions. The melt pool geometry is constant and the solidification front initially along the [001] orientation bows towards a direction given by the normal to the fusion boundary. Near the free surface of the melt pool a columnar to equiaxed transition occurs due to reduction in the thermal gradient in the liquid and increase in local growth rate.

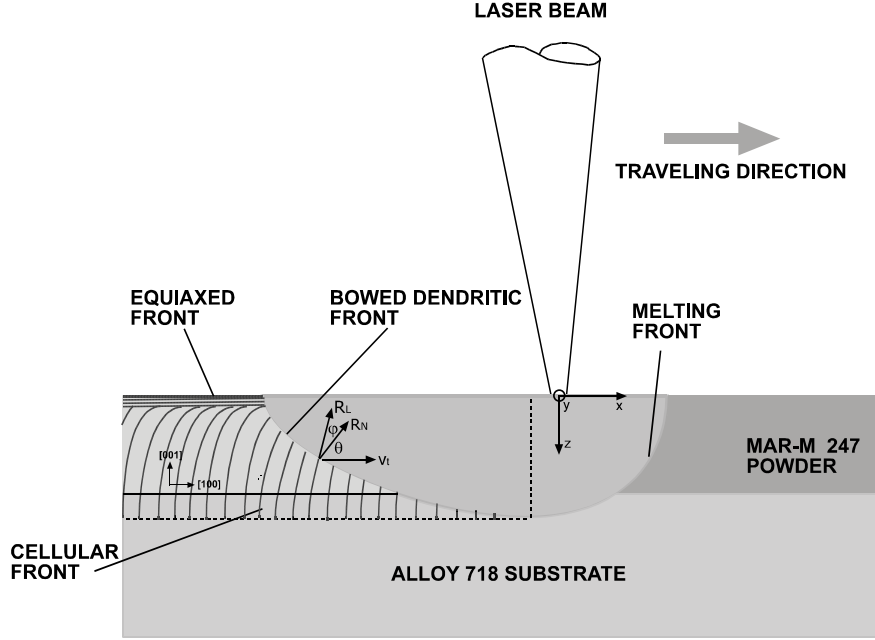


Figure 5. Schematics of the melting-solidification mechanisms encountered in SLM.

### Estimation of the thermal gradient in the melt

For a thick plate (i.e. semi infinite domain) the steady state solution to the three-dimensional heat transfer problem is predicted by the Rosenthal's solution<sup>2,6</sup>. From this solution, the thermal gradient at the fusion boundary  $G_L$  along the free surface of the melt pool (i.e.,  $y = 0$ ,  $z = 0$ ) behind the laser beam can be obtained by differentiation and corresponds to<sup>3,6</sup>,

$$G_L = \frac{2\pi K(T_m - T_o)^2}{P \cdot \eta} \quad (4)$$

Where  $K$  is the heat conductivity of the material,  $T_m$  is the melting temperature,  $T_o$  is the pre-heating temperature and  $\eta$  is the amount of laser power coupling into the material. At the free surface of the melt it can be assumed that  $R_L = v_t$  and according to Equation 3 at the critical condition, the following relationship is obtained,

$$P_{\text{critical}} = \frac{2 K(T_m - T_o)^2}{\eta \cdot f_{\text{critical}} \cdot v_t} \quad (5)$$

Therefore critical combinations of  $P$  and speed  $v_t$  will cause transition from columnar to equiaxed at the free surface of the deposit. From Equation 5, a decrease in  $P$  must be compensated by a corresponding increase in  $v_t$  to maintain dendritic growth up to the surface<sup>6</sup>.

## Experimental Procedure

Sample preparation consisted of coating a 2 mm thick Mar-M 247 mask with boron nitride spray. The coated mask was then clamped to Alloy 718 plates using a registration fixture (Figure 4). Mar-M 247 powder is mixed with isopropyl alcohol to form a slurry that was deposited in the trough of the mask using a pipette and was dried. The mask-substrate registration fixture was then placed inside the processing chamber. A  $10^{-5}$  Torr vacuum was applied to the chamber before back filling with inert-reducing gas (argon - 4% hydrogen). Pre-heat by means of a radiant shield was applied in order to degas the powder after processing and to alter the thermal gradient in the liquid during the laser processing. A focused Nd:YAG laser beam with a spot size of 0.25 mm was then selectively raster scanned along the mask trough at constant scan speed. Laser power was ramped down in certain experiments as part of an open-loop control scheme. The deposits were laid parallel to the rolling direction of the substrate plate. To be then sectioned across and along the longitudinal axis and polished according to the standard metallographic preparation procedure. Marble's reagent was used to etch the specimens and reveal the microstructure features. Table 1 shows the process parameters used in forming single layer - single track deposits.

Table 1. Process parameters of selective laser melting deposits.

Specimen ID	Power P [W]	Scan speed $v_s$ [mm/s]	Travel speed $v_t$ [mm/s]	Pre-heat $T_o$ [°C]	Energy density [J/cm <sup>2</sup> ]	$R_L = v_t$ [in/sec]	$G_L$ [°F/in]
21	235	524	1.4	25	179	0.0572	64346
31	235	524	1.4	700	179	0.0572	15323
51	125	205	1.0	775	244	0.043	22482
55	250	444	1.8	835	188	0.073	9572

## Results and Discussion

Figure 6 shows a log  $R_L$  versus  $G_L$  plot where a  $G_L/R_L$  ratio of 38000 °Fs/in<sup>2</sup> has been graphed (continuous line). This  $G_L/R_L$  ratio value is of most interest as it determines the columnar to equiaxed transition zone for all nickel base alloys<sup>8</sup>. The values of  $G_L$  were obtained from Equation 4 using the heat conductivity and melting point of Mar-M 246 from Ref. 9, i.e.,  $K = 0.4225$  W/in/°F @ 2000 °F and  $T_m = 2450$  °F. The laser coupling efficiency  $\eta$  was taken as 100%. According to this plot it can be seen that all specimens fall inside the columnar dendritic growth region away from the columnar to equiaxed transition boundary and therefore they should not have nucleated and grown equiaxed grains at the surface of the deposit. However, this observation does not hold as revealed by optical microscopy.

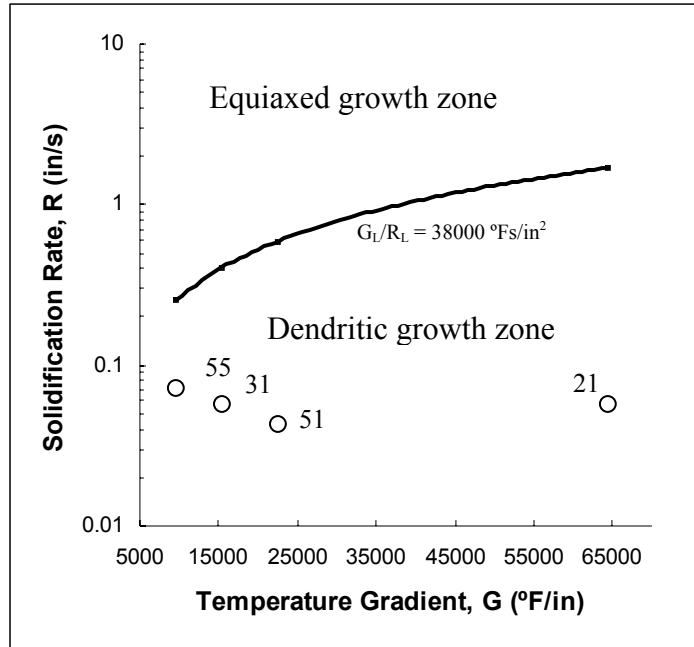


Figure 6. Solidification processing map for the SLM of Ni-base superalloy powder (Table 1 and Ref. 8).

From Figure 7 it can be seen by the overall shape of Specimen 21 that a low wetting angle occurred at the deposit-substrate interface. The width of the deposit at the interface is 1191  $\mu\text{m}$  and its center height is 1244  $\mu\text{m}$ . The upper surface of the deposit is round after solidification due to the non-wetting mask surface as well as a high surface tension at the center compared to the lateral sides. This indicates that high temperatures in the melt are experienced at the sides rather than the center of the melt pool. Figure 8 shows the narrow metallurgical bond achieved between the deposit and substrate. Cellular growth extends 264  $\mu\text{m}$  perpendicularly upwards from the interface and is then followed by a fine columnar dendritic growth along the [001] direction up to 471  $\mu\text{m}$ . Some polycrystalline columnar dendrites show a certain degree of mis-orientation from the [001] direction. The approximate primary arm dendrite spacing is 22  $\mu\text{m}$  and some porosity is also observed.

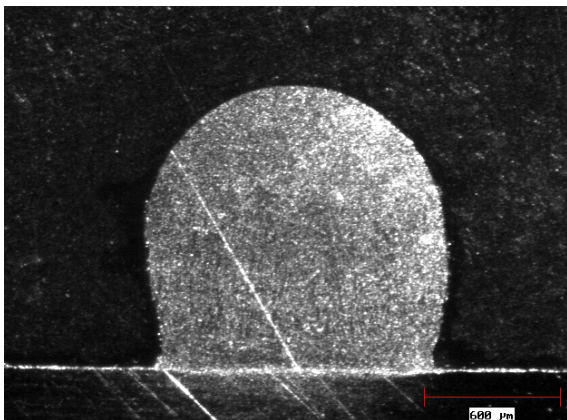


Figure 7. Macrograph of the cross-section of a Mar-M 247 deposit over Alloy 718 substrate corresponding to Specimen 21, 25x.

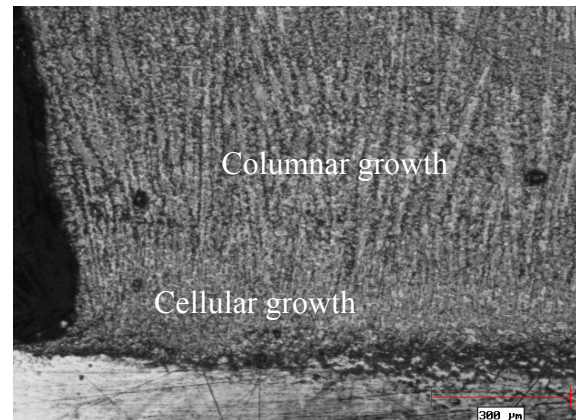


Figure 8. Micrograph of the cross-section of Specimen 21, showing the deposit-substrate interface, 100x.

From Figure 9 it can be observed that above the middle of the deposit the dendritic [001] growth tilts towards the [100] orientation. This may be caused by a change in direction of the maximum thermal gradient at the fusion boundary during solidification of the spherically shaped melt pool. The same microstructural description is observed in Figure 10, which corresponds to a deposit processed with the same laser parameters, but with a 700°C pre-heat. The microstructural features appear slightly coarser in size under the same magnification. At the apex of the deposit, equiaxed growth takes over due to a low thermal gradient in the liquid free surface and a high solute saturation favoring a large constitutional undercooling. Broken dendrite arms, unfused powder as well as oxide inclusion can be potent heterogeneous nucleation agents for equiaxed grains. The equiaxed zone at the surface of this deposit appears larger as the thermal gradients are reduced by the pre-heat condition.

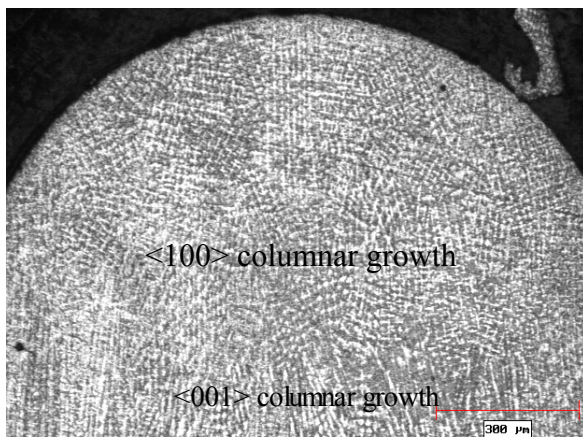


Figure 9. Micrograph of the cross-section of Specimen 21, showing the upper region of the deposit, 50x.

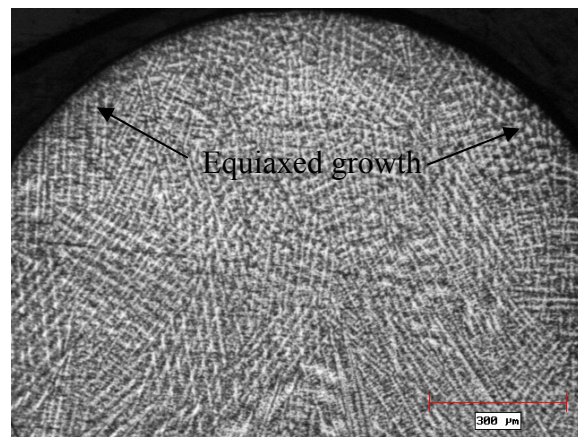


Figure 10. Micrograph of the cross-section of Specimen 31, showing the upper region of the deposit, 50x.

In Figure 11 a fusion zone of depth equal to 177  $\mu\text{m}$  can be seen in the substrate of Specimen 51 due to the 775°C pre-heating and lower laser traveling speed conditions. However, the laser power used in this deposit was reduced to a half the value used for Specimen 21. A cellular growth extends 57  $\mu\text{m}$  from the HAZ and it then turns columnar dendritic. In Figure 12 polycrystalline dendrites are clearly observed growing in the [001] direction up to an extension of 721  $\mu\text{m}$  above the substrate surface. The primary dendrite spacing corresponds to approximate 21.5  $\mu\text{m}$ .

Figure 13 shows Specimen 55 processed using an open loop power control scheme that ramped down the power from 250 W to 150 W as the specimen was deposited, keeping the laser beam traveling speed constant. At the cellular/dendrite interface a solidified polycrystalline dendritic structure region was achieved having a primary arm spacing of 16  $\mu\text{m}$ . Some porosity is also seen. From Figure 14 it can be observed how the polycrystalline dendrites experience a reorientation from the [001] direction towards direction of maximum thermal gradient at the fusion boundary.

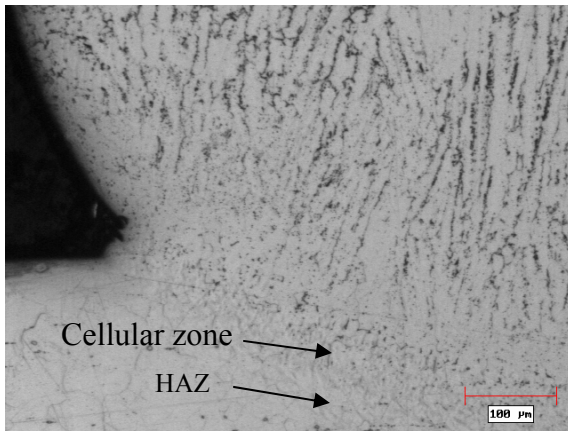


Figure 11. Micrograph of cross-section of Specimen 51, showing the deposit-substrate interface, 100x.

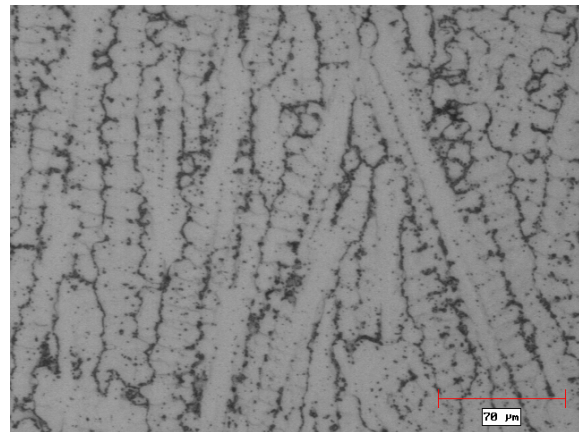


Figure 12. Micrograph of the columnar dendritic region above the cellular region in Specimen 51, 200x.

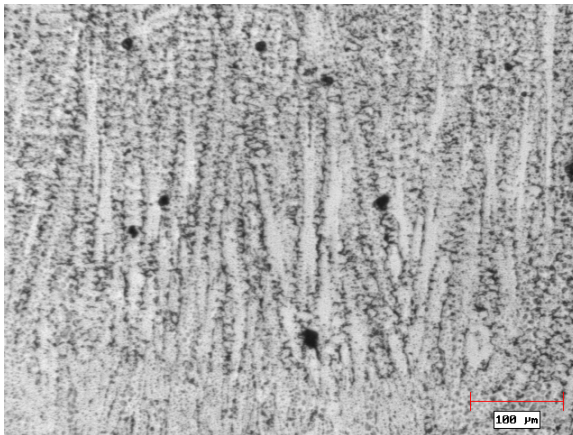


Figure 13. Micrograph of the cross-section of Specimen 55, showing polycrystalline dendrites above the cellular region, 100x.

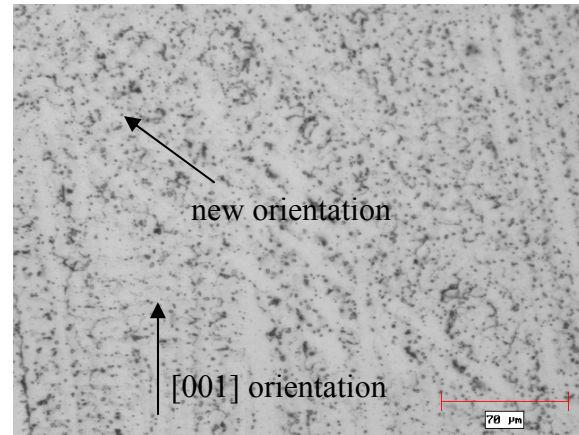


Figure 14. Micrograph of the longitudinal-section of Specimen 55, showing reorientation of dendrites, 200x.

Figure 15 shows a successfully SLM single-layer U-shape deposit processed with three sets of parameters for each region, namely: right track: 250-150 W,  $v_t = 1.65$  mm/s,  $v_s = 630$  mm/s; U-turn: P = 130 W,  $v_t = 0.92$  mm/s,  $v_s = 1260$  mm/s; left track: P = 150-200 W,  $v_t = 1.65$  mm/s,  $v_s = 630$  mm/s. Pre-heat was set to 700°C. The complete U-shape was laid using an open-loop laser power control.

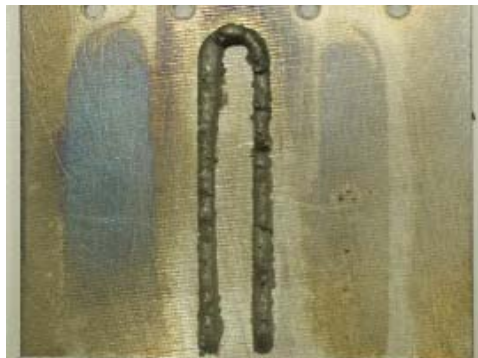


Figure 15. Single-layer U-shape deposit SLM laid using an open loop control scheme.

## Conclusions

Deposition of single layer – single track Mar-M 247 over Alloy 718 polycrystalline sheet was achieved successfully. U-shape single layers were also deposited taking advantage of an open-loop laser power control scheme.

Sound metallurgical bond were observed between the substrate and the deposit. A narrow cellular front solidified due to the high thermal gradient in the liquid and slow local growth rate.

Polycrystalline dendrites grow perpendicular to the substrate along the  $\langle 001 \rangle$  orientation up to half the height of the deposits as also reported in Ref. 5. It appears that the dendritic front then experiences bowing as the maximum thermal gradient at the fusion boundary rotates towards a  $\langle 100 \rangle$  direction as the free surface of the melt pool is approached. This indicates that the shape of the melt pool must have a spherical shape rather than a comet shape.

The measured primary dendrite arm spacing was found to be in the 16-22  $\mu\text{m}$  range. It had the same order of magnitude as the primary dendrite spacing found in laser claddings of Ni-base superalloy deposits reported in Ref. 5.

Near the free surface, columnar to equiaxed solidification transition occurs, likely due to the  $G_L/R_L$  ratio decrease. Solute is also rejected from the fusion boundary and its concentration builds up, increasing the degree of constitutional undercooling in the melt ahead.

It appears desirable to perform electron back scattered diffraction (EBSD) maps of the cross section of some deposits (e.g., Specimen 21) to verify the formation of equiaxed grains near the surface, as it is difficult to distinguish them from the reoriented columnar dendrites by means optical micrographs.

In order to extend the epitaxial dendritic  $\langle 001 \rangle$  growth further to the top of the deposit a comet-shaped melting pool is necessary. This requires a higher laser power input as well as higher laser beam traveling speed. However, an energy density in the range of 179-244  $\text{J}/\text{cm}^2$  must be met to achieved the required penetration depth. Moreover,  $P$  and  $v_t$  must be selected so that the  $G_L/R_L$  ratio, evaluated at the free surface of the melt pool, is less than or equal to the CET critical value for the Ni-base superalloy.

CMSX-4 single crystal substrates will be employed in future deposition experiments to observe the changes in microstructural evolution, specifically, the reorientation of the dendritic growth and the columnar to equiaxed transition.

## References

1. J.F. Ready, Ed. (1979): Lasers in Modern Industry. Society of Manufacturing Engineers.
2. W.M. Steen (1994): Laser Material Processing, 2<sup>nd</sup> edition, Springer Verlag.
3. M. A. Otooni (1998): Elements of Rapid Solidification, Springer Series in Materials Science 29, SprincerVerlag.
4. Suman Das *et al*, “Direct Laser Fabrication of a Gas Turbine Engine Component – Microstructure and Properties – Part I”, 10<sup>th</sup> Solid Freeform Fabrication Symposium, Austin Texas August 1998, 1-9.
5. M. Gäumann *et al*, “Epitaxial laser metal forming: analysis of microstructure formation”, *Mat. Sci. Eng. A*, 271(1999), 232-241.
6. O. Grong (1994): Metallurgical Modelling of Welding, Materials Modelling Series, The Institute of Materials.
7. D.A. Porter and K.E. Easterling (1992): Phase Transformations in Metals and Alloys, 2<sup>nd</sup> edition, Chapman & Hall.
8. M. McLean (1983): Directionally Solidified Materials for High Temperature Service, The Metals Society, London.
9. Metals Handbook, 9th edition, Vol. 3, Properties and Selection: Stainless Steel, Tools Materials and Special Purposes, Metals Park, Ohio.

## Acknowledgments

Funding for this project was provided by Rolls-Royce North America and the University of Texas at Austin.